Science Bulletin 66 (2021) 1176–1185

Contents lists available at ScienceDirect

Science Bulletin

journal homepage: www.elsevier.com/locate/scib

Article

Volatile organic compounds sensing based on Bennet doubler-inspired triboelectric nanogenerator and machine learning-assisted ion mobility analysis

Jianxiong Zhu [a,b,c,d], Zhongda Sun [b,c,d], Jikai Xu [b,c,d], Rafal D. Walczak [e], Jan A. Dziuban [e], Chengkuo Lee [b,c,d,f,*]

[a] School of Mechanical Engineering, Southeast University, Nanjing 211189, China
[b] Department of Electrical and Computer Engineering, National University of Singapore, Singapore 117576, Singapore
[c] Center for Intelligent Sensors and MEMS (CISM), National University of Singapore, Singapore 117576, Singapore
[d] NUS Suzhou Research Institute (NUSRI), Suzhou 215123, China
[e] Department of Mircroengineering and Photovoltaics, Wroclaw University of Science and Technology, Wroclaw 50-370, Poland
[f] Integrative Sciences and Engineering Programme (ISEP), National University of Singapore, Singapore 119077, Singapore

ARTICLE INFO

Article history:
Received 17 December 2020
Received in revised form 4 February 2021
Accepted 15 March 2021
Available online 23 March 2021

Keywords:
Machine learning
Volatile organic compounds
Ion mobility
Triboelectric nanogenerator
Plasma discharge

ABSTRACT

Ion mobility analysis is a well-known analytical technique for identifying gas-phase compounds in fast-response gas-monitoring systems. However, the conventional plasma discharge system is bulky, operates at a high temperature, and inappropriate for volatile organic compounds (VOCs) concentration detection. Therefore, we report a machine learning (ML)-enhanced ion mobility analyzer with a triboelectric-based ionizer, which offers good ion mobility selectivity and VOC recognition ability with a small-sized device and non-strict operating environment. Based on the charge accumulation mechanism, a multi-switched manipulation triboelectric nanogenerator (SM-TENG) can provide a direct current (DC) bias at the order of a few hundred, which can be further leveraged as the power source to obtain a unique and repeatable discharge characteristic of different VOCs, and their mixtures, with a special tip-plate electrode configuration. Aiming to tackle the grand challenge in the detection of multiple VOCs, the ML-enhanced ion mobility analysis method was successfully demonstrated by extracting specific features automatically from ion mobility spectrometry data with ML algorithms, which significantly enhance the detection ability of the SM-TENG based VOC analyzer, showing a portable real-time VOC monitoring solution with rapid response and low power consumption for future internet of things based environmental monitoring applications.

1. Introduction

Volatile organic compound (VOC) is an organic chemical with a high vapor pressure at room temperature, making it easy to evaporate or sublimate in the compound molecules to the surrounding air due to its low boiling point [1–3]. Owing to the high demand in manufacturing, VOC plays a paramount role in various industrial fields, including chemistry, agriculture, and semiconductors, resulting in a large amount of VOC gas by-products existing in the working and living environment. However, some VOCs are harmful to the environment, and long-term exposure to these VOC gases causes health issues, i.e., sensory irritation and chronic diseases. Thus, the detection technology of VOCs with high sensitivity, good selectivity, and fast response is indispensable for the security monitoring of the industrial environment and personal healthcare applications [4]. Current commercial VOC sensors and analyzers are commonly based on the mechanisms of oxide semiconductor, optics, electrochemical, etc. [5–14], which are typically developed for a certain range of VOC species and concentration, and limits in response speed and selectivity. Besides, the conventional plasma analyzers are bulky and operate in strict environmental conditions high temperature and low pressure, restricting their applications in the internet of things (IoT) sensing framework, where small sensor nodes operating in normal indoor/outdoor environments with low power consumption are preferred.

The ion mobility-based method is a well-known analytical technique for identifying and quantifying gas-phase compounds to implement the fast response detection for various species, which has been widely applied in areas such as process and quality control, food quality, medical diagnostics, biology, security, and military purpose [15–20]. It is a method of characterization by

* Corresponding author.
E-mail address: elelc@nus.edu.sg (C. Lee).

https://doi.org/10.1016/j.scib.2021.03.021
2095-9273/

various ion mobility patterns based on different gas compositions. To improve the sensing ability, different power sources, including ultraviolet light and β-radiation, have been adopted to ionize different kinds of molecules [21,22]. However, these external ionized power sources increase the cost and instability of the whole sensing system, and the strict constraints of the operating environment (e.g., vacuum or low pressure) dramatically restrict its industrial development [23–25]. Moving forward to the wireless sensing network under the IoT framework, small sensor nodes with a portable power source that can operate in the normal environment have become the new trends in ion mobility spectrometry sensing [26–29]. In this regard, with the coupling of triboelectric and electrostatic induction, the triboelectric nanogenerator (TENG) (first proposed in 2012) can harvest energy from various vibration sources [30–42] and produce high voltages without any sophisticated electronics [43–56]. TENG also presents its universal adaptability to all physical and chemical sensing scenarios with a self-powered strategy [57–67]. With the achievable output power from TENGs, the contact electrification-based gas sensor for VOCs was obtained with ability of power-free and highly selective gas sensing [68–72]. However, the existing TENG gas sensor (contact electrification-based) shows dramatically sensing limitation in real applications due to its instability output voltage and slow response (>100 s). To date, no persuasive research has been conducted based on the advantages of TENG-induced (portability and high-voltage output) plasma ion discharge for VOC detection [73–85].

In addition, with the development of the fifth-generation (5G) cellular network technology, artificial intelligence (AI)-enabled data analytics can be conducted at the cloud server to realize new artificial intelligence of things (AIoT) technology, where distributed low-cost and small sensor nodes collect sensory information and send them wirelessly to the cloud for machine learning (ML) assisted data processing and analysis [86–92]. Therefore, not only the power consumption but also the size of sensors are significantly reduced at the sensor nodes. The ML-enhanced method has been proven as an efficient tool to realize fast and high-accuracy gas recognition by extracting their specific features automatically from the sensing output with ML algorithms, saving a lot of manual interpretation and real-time calculation costs. Besides, ML provides a possibility to analyze and distinguish complex VOC gas mixtures. With the future 5G and AIoT technologies, the demand for self-powered ML-enhanced VOC sensors will increase in both the industrial and personal healthcare applications, where small portable real-time VOC-monitoring sensors with rapid response, high accuracy, and low-power consumption are needed.

Based on the above considerations, we proposed an ML-enhanced self-powered ion mobility sensing method with multi-switched TENG as the power source for various VOC species detection, i.e., methanol, ethanol, acetone, and isopropyl alcohol (IPA). This method shows the advantages of portable, self-powered, and fast response, and has no strict constraints of the operating environmental conditions compared with the conventional gas analyzer. High voltage was easily obtained and sustained by the special multi-switched manipulation of the TENG device based on charge accumulation mechanism, whose output voltage was further leveraged with a special type of tip-plate electrode configuration to obtain the plasma discharge of various VOC molecules. Based on the unique features, i.e., the number of peaks, frequency, and amplitude, of the ion discharging patterns, different VOCs can easily be identified. To further improve the VOC detection accuracy, a customized ML-enhanced tool was well developed to classify different VOC concentrations automatically based on specific features extracted by ML algorithms. It demonstrates that the proposed multi-switched manipulation platform enables the detection of multiple gas species by analyzing the corresponding time-domain ion mobility spectrometry with an ML-enhanced tool for fast and early VOC detection under on-strict environmental conditions.

2. Experimental

Three types of multi-switched manipulation of triboelectric nanogenerator (SM-TENG) were fabricated with a unit of contact friction area 10, 24, and 49 cm^2, respectively. The SM-TENG contains the bottom fixed plates (dielectric "A" and "C") and the top pair of movable plates (dielectric "B" and "D"). The materials of the triboelectric dielectric plate were poly(methyl methacrylate) (PMMA) and fluorinated ethylene propylene (FEP), respectively. The dielectric "A" and "C" are PMMA or polytetrafluoroethylene (PTFE), and the top movable pair of plates dielectric "B" and "D" are FEP. Notably, the triboelectric polarity materials (PMMA and FEP) in charge distribution are extremely large. The charge property distribution PMMA material is positive in series, whereas FEP or PTFE is triboelectric negative [93]. The PMMA dielectric presented positive surface charges when it contacts with FEP (negative charges) in operation. The multi-switched were produced by nickel conductive porous cloth due to mechanical robustness with "on" or "off". For the convenience of the fabrication to SM-TENG, the connection wires were made of nickel textiles. The substrate of the SM-TENG was made of an acrylic plate, which was cut by a laser cutting machine. The different thickness of the PMMA film was chosen as 1, 2, and 3 mm, respectively. Finally, the entire component was assembled to form the SM-TENG. The FEP and PTFE films are of ~220 and ~300 μm thicknesses, respectively. Because of the need for mechanical robustness and system integration, the electrode attached to the backside of the dielectric film was made of nickel conductive textile as well. The gas pre-mixture chamber was designed for the mixture of the VOCs species. The calibration sensor was used to identify the specific concentration of the mixture gas with different VOCs. The mass flow controllers (MFCs) were connected to the VOCs gas measurement chamber to provide the inlet mixture of VOC gases. To improve the accuracy of the VOC concentration, the gas chamber was well-sealed during the operation. The SM-TENG was used to provide the high-voltage power source for the needle-plate electrode configuration. The oscilloscope was connected to the plate electrode collector to record the dark current response during the sliding of SM-TENG.

3. Results and discussion

3.1. Ion mobility and multi-switched manipulation of TENG for ML-enhanced VOCs

Gases consisting of particles (molecules or atoms) are always in random motion, which surround human beings in a dynamic balance state. However, VOCs from waste materials are harmful to the human body, easily resulting in eye itching, heartbreak, or headache. This situation is severe for those in chemistry or materials research laboratories (Fig. 1a), where plenty of organic chemistry solvents evaporating from beakers can result in potential risks. To identify the VOCs in such scenarios, the phenomenon of ion mobility from the plasma discharge meets the requirement of fast detection and convenience. The sensing mechanism based on the drift time of ion mobility is illustrated in Fig. 1b. Various VOC species and their concentrations can be well-identified based on the transient dynamics of ion mobility patterns, which come from the weight and volume of different ions in drift. To reach the high-voltage output without any external battery and motivated by the logic of the charge accumulation from the natural world (such as the lighting), SM-TENG was developed based on the Bennet dou-

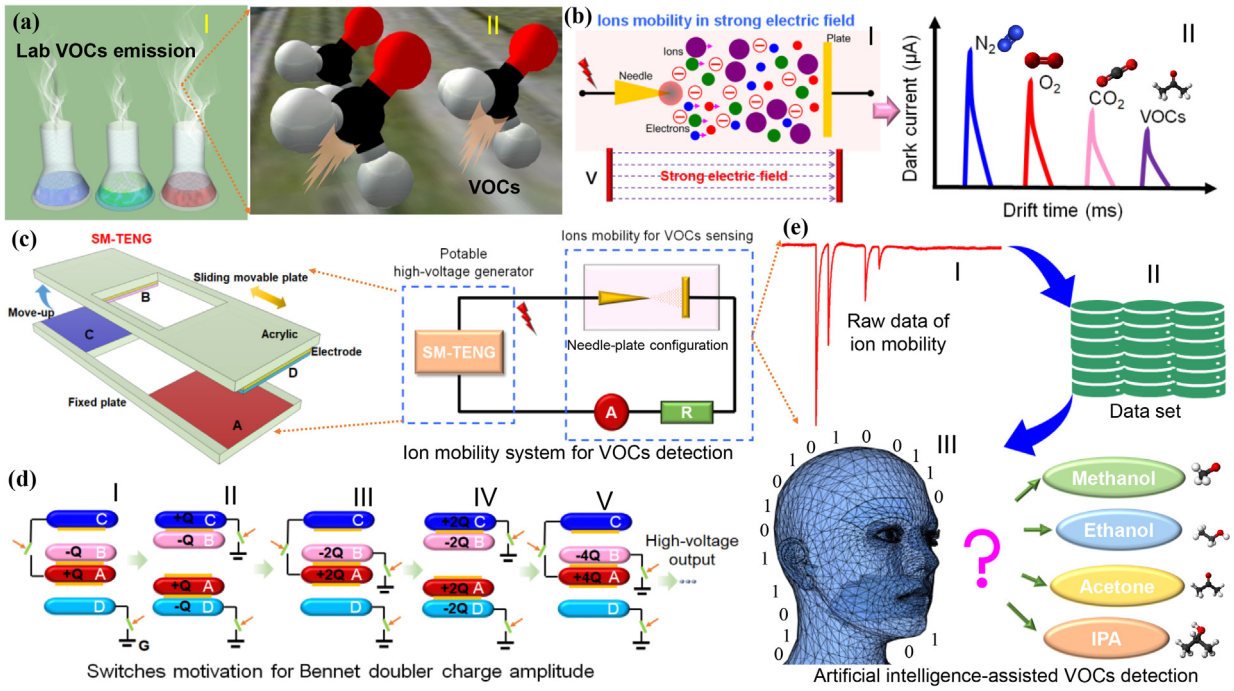

Fig. 1. (Color online) Machine learning (ML)-enhanced volatile organic compounds (VOCs) analyzer using ion mobility from multi-switched manipulation of a triboelectric nanogenerator (SM-TENG). (a) The source of VOCs in lab and VOC molecules. (b) The ion mobility of VOCs in a strong electric field and their drift time. (c) 3D diagram of SM-TENG and the ion mobility for VOC detection. (d) The operation mechanism of the Bennet doubler based on multi-switched manipulation for charge accumulation. (e) ML-enhanced ion mobility for VOC detection.

bler. Afterward, leveraging the output voltage in a special type of tip-plate electrode configuration, a wide range of VOC molecules detection using ion mobility from SM-TENG was proposed (Fig. 1c). The ion mobility characteristics in the VOC chamber present the different transient phenomena with a variety of VOC species and their concentrations. The discharge phenomenon in nature is a complex process involving the dark, glow, and arc discharges (Fig. S1 online). The dark discharge shows a much sustainable output than the glow and arc discharges during the VOC detection due to its stable output and low power consumption.

The operations of multi-switched manipulation ("on" or "off") in time sequence are explained to describe the working mechanisms of the Bennet doubler (Fig. 1d) [94,95]. Both triboelectric effect and electrostatic induction generate initial charges onto dielectrics "A" and "B", and electrode "B", which is located at the backside of dielectric "B" will be charged with the same quantity but opposite charges. Owing to the surface interface effect of the triboelectric dielectric materials and the charge transfer in "C" and "D", the multi-switches will operate between "on" and "off" action, resulting in a continuous charge accumulation onto the electrode "A". Thus, the charge manipulation in the time sequence would convert the mechanical energy to electric energy by leveraging the accumulated charge onto dielectrics "A" and "B" from the ground. From the sliding and multi-switched manipulation, the high-voltage output is easily obtained rather than investigating the selection of materials (conventional TENG devices, as shown in Figs. S2 and S3 online). Notably, the Bennet doubler provides a unidirectional current flow for charges accumulation resulting in a high-voltage output. By leveraging the needle-plate configuration to discharge, a dramatic pattern difference of the transient dark current responding to VOCs is achievable. Further, to better identify the VOC molecules using ion mobility analyzer response, an ML-enhanced tool (learn the uniqueness of different VOC molecules from a range of parameters, i.e., number of peaks, frequency, and amplitude) was adopted for augmented detection (Fig. 1e). Thus, according to the pattern of the dark current and the leverage in a special type of tip-plate electrode configuration from SM-TENG, the detection of a wide range of VOCs, such as methanol, ethanol, acetone, and IPA, using an ion mobility analyzer was achieved for early and fast detection at room temperature (RT).

3.2. Working mechanism and electrical performance of SM-TENG

Inspired by the mechanism of the Bennet doubler, the in-plane mechanical structure of the SM-TENG was achieved through the back and forth sliding and switches in a time sequence operation (Fig. 2a). Notably, the backside of the dielectric materials ("A", "B", "C", "D") was pasted with conductive layers (nickel conductive textile was chosen due to its mechanism robustness). The initial charges of the dielectric materials are generated by the triboelectric friction. As shown in Fig. 2a(I), the electrode layers of dielectric "C" and "D" will attract charges from the ground due to electrostatic induction and triboelectric effect. The intermediate state is the function where multi-switches are "off" to keep a separation by the air (Fig. 2a(II) and a(IV)). With further sliding of the movable plate, the electrodes on the backside of dielectric "D" and "B" will obtain more charges from the ground to balance the charges due to electrostatic induction of their dielectric films. As the movable plate moves back to the initial state, more charges will accumulate on "A" and result in a high-voltage output (from 1 to 2 Q). With more operation cycles to SM-TENG, the charges on dielectric "A" will multiply with increasing operation cycles (from 2 to 4 Q, and more). Electrode "A" will continuously keep the charges accumulation for high-voltage output until the limit of air breakdown. Thus, the ultrahigh voltage output can be easily achieved on the basis of the multi-switch manipulation in a time sequence operation, which is almost impossible for conventional TENG.

The characterization results of the electrical performance of different dielectric materials, the open-circuit voltage (V_{oc}) and open-circuit charge (Q_{oc}) vs. different contact areas of the same (FEP vs.

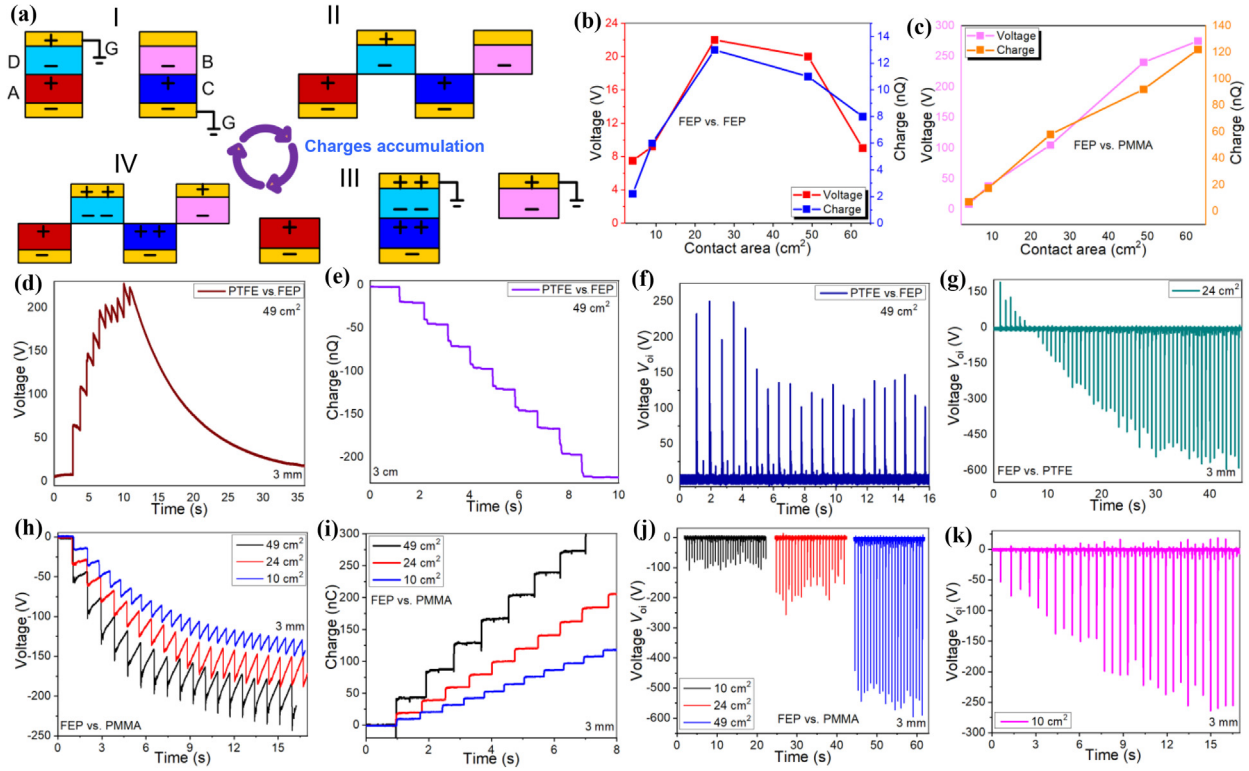

Fig. 2. (Color online) SM-TENG and its electrical performance. (a) Schematic illustration of the working principle of SM-TENG. (b) Electrical performance of FEP vs. FEP with different contact areas. (c) FEP vs. PMMA with different friction areas. (d) V_{oc} from PTFE vs. FEP to present an unstable output. (e) Q_{oc} from PTFE vs. FEP. (f) V_{oi} from the oscilloscope of 100 MΩ to describe the output performance. (g) Charges in reversal polarity phenomena between FEP and PTFE. (h) V_{oc} from FEP vs. PMMA. (i) Q_{oc} from FEP vs. PMMA. (j) V_{oi} from oscilloscope of 100 MΩ. (k) Operation from initial to a saturation status.

FEP) and different triboelectric polarity materials (FEP vs. PMMA) can be seen in Fig. 2b, c, respectively. A programmable electrometer (Keithley model 6514) was used to conduct those parameters (V_{oc} and Q_{oc}). The result shows that the same triboelectric material (FEP vs. FEP) results in low charge transfer efficiency and small voltage output. The reason for this phenomenon could be the charge saturation during the friction. However, these materials can still obtain a small value of initial charges even with the same triboelectric materials. The electrical performance of the other potential material, PTFE is shown in Fig. S4 (online), where PTFE vs. PMMA exhibits much better electrical performance than PTFE vs. FEP. If with the same or similar triboelectric materials, the charges and the instantaneous voltage from the surface of the materials would be a small value and in strange phenomenon based on our observation. The obtained or loss charges might be from the surface nanostructure with the triboelectric effect in perturbation, which results in a small value and strange phenomenon. If Figs. 2b, c and S4a, b (online) are in the same *Y* scale, the curves from Figs. 2b and S4a (online) would almost be in a flat line. The same or similar triboelectric materials produced a quite small charge output. An unstable output voltage was obtained from similar triboelectric materials (PTFE vs. FEP) in SM-TENG (Fig. 2d, e). The reason, as mentioned above, might be the low efficiency of charge transfer between these similar triboelectric materials (Fig. 2f). V_{oi} was obtained from the oscilloscope with 1 MΩ resistance (close to the plate side from the needle-plate configuration). Instability and the charge in reversal polarity phenomena between FEP and PTFE are shown in Fig. 2g, and its zoom-in is shown in Fig. S5 (online). To describe the working performance of the SM-TENG, the voltage and peak power by changing load resistance are shown in Fig. S6 (online). Theoretically, charges on electrode "A" can accumulate infinitely without limit. However, it shows a maximum voltage output to the SM-TENG due to the air breakdown and the maximum charge storage ability of dielectric materials. To further investigate the electrical property of the chosen material, the measurement of V_{oc}, and accumulative Q_{oc} of the SM-TENG were conducted, and the results are shown in Fig. 2h, i. 45 nC and ~60 V were obtained for a cycle of sliding operation of the SM-TENG with an area of 49 cm^2. A larger contact area of the SM-TENG can induce more charges and result in a larger output voltage for each cycle (Fig. 2j). SM-TENG also presents good directional charge flow during the sliding operation. As D/B repeatedly contacts and releases to A/C dielectric materials, triboelectric charges get higher until charge saturation, which means the extra charge dissipation in air or discharge onto the opposite materials through the air. Normally, the stable output voltage comes after 5–6 times or more periodic sliding from our observation. When it comes to saturation status, it assumes a stable status in needle-plate configuration for plasma discharge. In addition, the detailed information about the operation process of the SM-TENG from the initial to the saturated output is shown in Figs. 2k and S7 (online).

3.3. Performance optimization of SM-TENG

Based on the theory of the triboelectric and electrostatic effect, the size of the contact area and the thickness of the dielectric layer can be optimized to meet a high-output voltage (Fig. S8 online). The result shows that almost one time higher output voltage was obtained with a thickness of 1 mm than that of 3 mm. The numerical simulations for those factors were conducted and the corresponding output electrical signals are shown in Fig. 3. The SM-TENG presents good repeatability in charge accumulation (Fig. 3a–c). We also observe that the charges are in a unidirectional

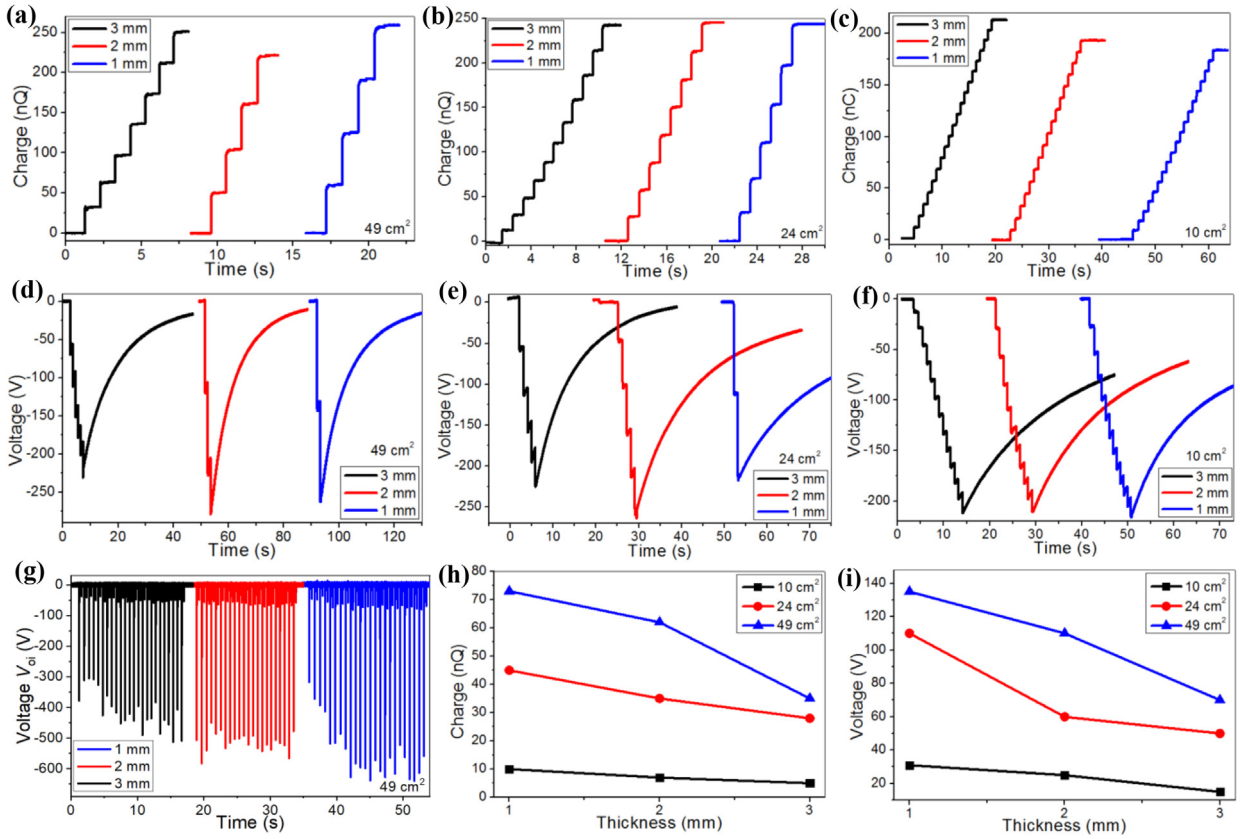

Fig. 3. (Color online) Performance optimization of SM-TENG. (a–c) Accumulative Q_{oc} from 49, 24, and 10 cm^2, respectively. Each increasing step comes from a cycle of sliding in back and forth. (d–f) V_{oc} from 49, 24, and 10 cm^2, respectively. (g) V_{oi} from oscilloscope of 100 MΩ. (h) Q_{oc} vs. the thickness of the triboelectric dielectric. (i) V_{oc} vs. the thickness of the triboelectric dielectric.

flow (step increase) during the sliding operation. It means that the multi-switches work well for charge accumulation. If the sliding stops, the output voltage would decay due to the discharges (Fig. 3d–f). SM-TENG with a 1 mm dielectric layer can achieve two times higher V_{oc} than that of 3 mm. The voltage V_{oi} from the SM-TENG collected by an oscilloscope of 100 MΩ input impedance presents ~1.5 times higher voltage than the device with the smallest contact area shown in Fig. 3g. Furthermore, the thinner thickness of the dielectric film, the higher the output voltage, and the more accumulative charges from the SM-TENG would be obtained (Fig. 3h, i). Higher power of 75 nC and 135 V from a cycle of operation in sliding was obtained from our observation. Thus, this information provides an engineering solution to improve output voltage with optimization in dielectric layer thickness and the contact area.

3.4. Ion mobility analyzer and VOC mixture detection

With the high-voltage power from SM-TENG and its further leverage in a special type of tip-plate electrode configuration, a wide range of VOC molecule detection based on the ion mobility phenomenon was proposed (Fig. 4a). Notably, the injected VOC gases in the gas chamber could be either pure or mixed gases. The ion mobility characteristic in the form of the dark current with certain tip-plate electrode configurations presents different transient phenomena with various VOC species and their concentrations, which could have the potential for fast and early VOC detection. In this study, VOC gases were well pre-mixed in the gas chamber before being injected into the needle-plate electrode configuration. The unique patterns of the ions in the complex gas environment are shown in Fig. 4b, c. Video S1 (online) depicts the operation to get the ion mobility patterns. The high concentration (VOCs, acetone) dramatically damped the drift time compared with the low concentration. The optical image of the needles and the tips is shown in Fig. S9 (online). The schematic diagram of the ion discharges in VOCs and the corresponding dark currents with drift time is shown in Fig. S10 (online).

To identify the sensing feasibility of mixed VOCs (Fig. 4d), two different VOCs (i.e., ethanol and acetone) were well mixed in the pre-mixture chamber for demonstration. If with other waste chemicals, the pattern of ion mobility would be changed as well. Owing to the complex molecule-structure of both VOCs, the two VOCs might present a cluster phenomenon but could still be identified on the basis of our observations. With those VOC mixtures, different kinds of patterns were measured (Fig. 4e, f). We assumed that these similar patterns predicted the strong cluster of those similar VOCs. More cycles of the low concentration measurement are shown in Fig. S11a (online). An in-depth study of the dark current pattern of ion mobility based on three different mixed VOC gases (i.e., methanol, ethanol, and acetone) is shown in Fig. 4g, and the unique dark current patterns from the mixed VOCs are shown in Figs. 4h, i and S11b (online). The reason for choosing these three VOCs lies in the characteristic of one carbon of VOC (methanol), two carbons of VOC (ethanol), and three carbons of VOC (acetone), which presented that the ion mobility analyzer is suitable for all kinds of VOCs. VOC molecules would be much easier to cluster due to the density of the VOCs. The patterns of dark current, as well as concentrations of VOCs, can also be identified.

3.5. ML-enhanced ion mobility analyzer for VOC detection

The drift time of the ion would be markedly different in discharge due to the different weights and volumes of the molecules (Fig. 5a). Meanwhile, the large volume of the molecules would be a

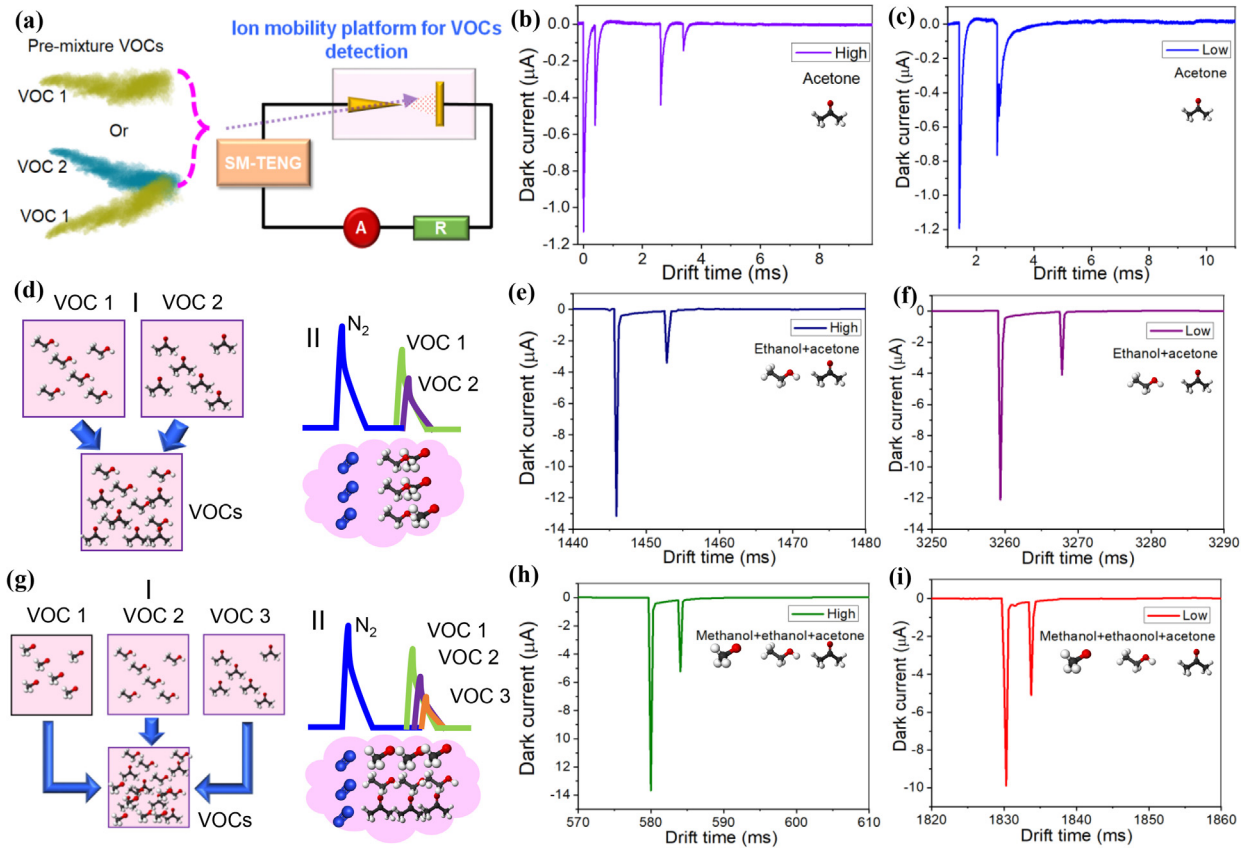

Fig. 4. (Color online) VOCs and VOC mixture detection using ions mobility analyzer from SM-TENG. (a) Ion mobility analyzer platform for VOC detection using single or mixed VOCs. (b, c) The dark current pattern of high and low concentrations, respectively. (d–f) Two kinds of mixed VOCs and their ion mobility patterns, high and low concentration, respectively. (g–i) Three kinds of VOCs and their ion mobility patterns, high and low concentrations, respectively.

damper to impede the motion of the small molecule, resulting in the damping effect. Here, gas ions including air molecules and VOCs are frequently colliding during the operation (almost no net loss of energy from the collisions due to elastic). To improve the sensing performance of VOCs based on the mechanism of ion mobility in SM-TENG, the ML-enhanced method was adopted to enhance VOCs sensing (Fig. 5b). By using the ML tool, the ion mobility pattern would be easily identified for different VOC concentrations. The ML algorithm used is a one-dimensional convolution neural network (1D-CNN), which can automatically extract features from different VOC output and provide a powerful classification between different categories. The architecture of the 1D-CNN we used is shown in Fig. S12 (online). Notably, the ion mobility in the air pressure was measured (Fig. 5c). The molecules of O_2 and N_2 can be identified from the ion mobility system from our observation. Thus, it is possible to distinguish the other chemical molecules due to molecule weight in motion between the needle-plate configuration (heavier than O_2 and N_2). If with the other waste chemicals (heavier than O_2 and N_2) in a practical laboratory or factory environment, the pattern of ion mobility would be changed as well. To demonstrate the effect of the ML-enhanced identification of ethanol and IPA in the aspect of the dark current pattern, three different concentrations with typical dark current patterns were described (Fig. 5d, e). A higher concentration of the VOCs will induce a longer drift time (3 ms of high concentration to 0.5 ms of low concentration for ethanol, and 6 ms of high concentration to 1 ms of low concentration for IPA). With the ML tool, the recognition accuracy of different concentrations can reach 48.3% (Fig. 5f), which is reasonable considering the properties of gas molecules. Each category has 50 samples, where 42 samples are used for training and 8 samples for testing. The data length of each sample is 16,000. This ML-enhanced identification method provides quick and automatic VOC recognition, which saves a lot of manual interpretation and real-time calculation costs. It is interesting that the environment and the median IPA show the highest accuracy in ML. The reason for this high accuracy might be the damping of VOCs and various molecule structures according to weight properties, which results in higher accuracy in ML. To identify all kinds of VOC gases, typical VOCs had been chosen for the measurement: VOCs with one carbon (methanol), two carbons (ethanol), and three carbons (acetone). Further, even with the same VOCs carbons (acetone and IPA), the ion mobility system can still distinguish between them based on our observations.

For an in-depth study of the influence of the needle-plate electrode configuration on ion mobility, we experimented with different gap distances for VOC discharge. To quantify the discharge with the gap distance, the numerical relationship between the gap of the needle-plate and the output voltage was investigated (Fig. S13 online), indicating that a smaller SM-TENG device can induce a lower output voltage. Result also shows that a shorter distance of the air gap of the needle-plate configuration can induce a stronger discharge in the gas chamber (~3 times more). To validate the robustness of the ML-enhanced method with various needle-plate electrode configurations, different air gaps (0.5 and 1.5 mm) were considered (Fig. 6a). The drift time of the ion in a wide air gap is much longer than that of the narrow air gap (Fig. 6b). The ion mobility in the air was tested (Fig. 6c). Owing to the discharges of various VOC species and their different concentrations in the gas chamber, the ion mobility patterns are different (Fig. 6d–f). The ion mobility patterns show significant differences

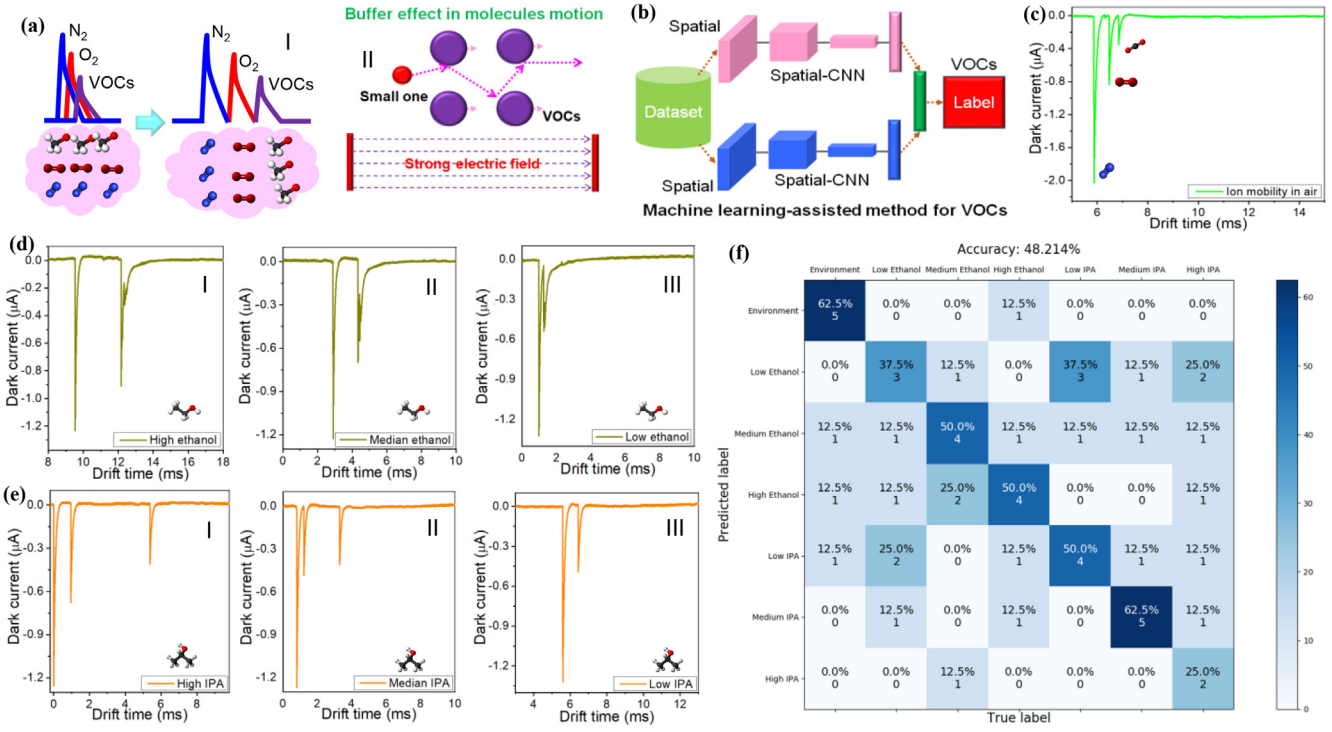

Fig. 5. (Color online) ML-enhanced ion mobility analyzer for VOC concentration detection. (a) Different ions and buffer effects in directional motion. (b) The ML-enhanced method for VOCs. (c) The ion mobility in the air. (d) Typical pattern of dark current to ethanol, 2970, 1320, and 660 parts per million (ppm), respectively. (e) The typical pattern of the dark current to IPA, 1300, 800, and 400 ppm, respectively. (f) ML-enhanced results of different concentrations to ethanol and IPA, respectively.

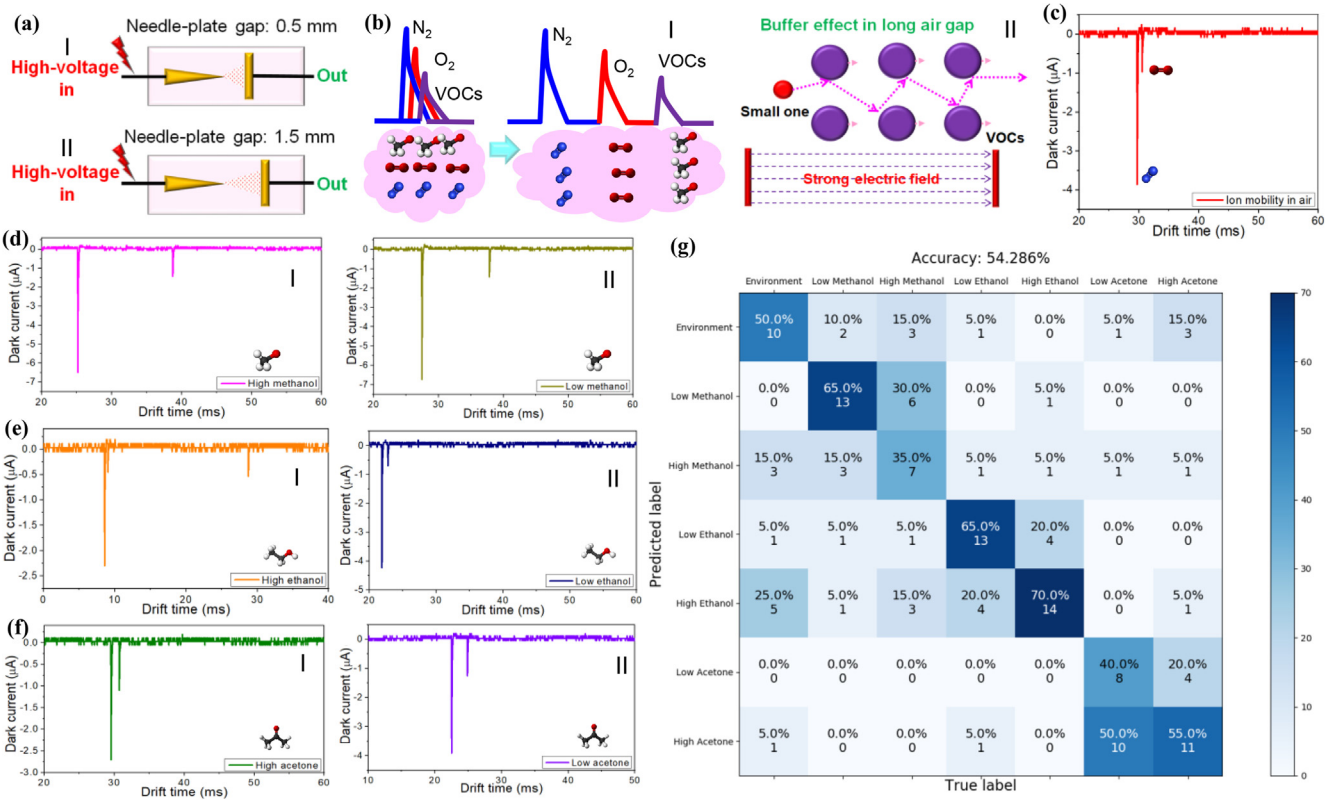

Fig. 6. (Color online) The gap distance of the needle-plate electrode configuration for ML-enhanced ion mobility identification. (a) Two different air gaps of the needle-plate configuration. (b) The ions and buffer effect in directional motion in a long-distance air gap (~2 mm). (c) The ion mobility in the air with ~2 mm gap. (d) Typical pattern of dark current to methanol, high and low concentration. (e) Typical pattern of dark current to ethanol, high and low concentration. (f) Typical pattern of dark current to acetone, high and low concentration. (g) ML-enhanced results of different concentrations of methanol, ethanol, and acetone, respectively.

Table 1
Comparison of the advantage of VOCs detection in our work and the current state-of-the-art.

Items	Materials and mechanism	Response & recovery	Kinds of VOCs	Sensing environment	Mixture detection	Portability	External power
Ref. [96]	Pd/SnO_2 Chem-iresistive	21 s, 230 s	Ethanol or acetone	250 °C	No	Yes but inconvenient	Yes
Ref. [97]	rGO/WO_3 Chem-iresistive	14 s, 40 s	Acetone or methanol	RT	No	Yes but inconvenient	Yes
Ref. [98]	Molybdenum disulfide (MoS_2) Chem-iresistive	10 min, not mentioned	Toluene, hexane, ethanol, and acetone	RT	No	Yes but inconvenient	Yes
Ref. [99]	rGO Chemiresistive	120 s, 176 s	Ethanol, nonanal, and ethylbenzene	RT	No	Yes but inconvenient	Yes
Ref. [100]	Resonant cantilever	60 s, 5 min	Aniline or acetic-acid	RT	No	Impossible	Yes
Ref. [23]	Plasma discharge	<1 s	Multi-compounds but without Concentration	70 °C	Yes	No due to bulky	Yes and > 3 kV
Ref. [3]	UV of ion mobility	<1 s	Methanol, ethanol, acetone, ethyl acetate, diethylamine	96 °C and 700 mbar	No	No due to bulky	Yes and >3 kV
Ref. [101]	UV of ion mobility	<1 s	Acetone, toluene, butanone	120 °C	No	No due to bulky	Yes and >3 kV
Our work	Plasma discharge	20 ms, 20 ms	Methanol, ethanol, acetone, and IPA	RT and air pressure	Yes	Yes	No

between different VOCs, such as methanol, ethanol, and acetone. With the ML, the waste chemical concentrations of VOCs can easily be identified based on their unique patterns (54.286% average). The highest accuracy (65% and 70%, respectively) can be obtained on ethanol due to the strong sense of its unique molecule structures (Fig. 6g). Notably, we measured 100 samples of data for each category. The data length of each sample is 16,000. Then we randomly chose 80 samples of each category for training and 20 samples for testing to assess the performance of the proposed ML tool on distinguishing the different VOC species and their concentrations. Now, the data set has 700 samples, and the number is relatively acceptable for a four-layer 1D-CNN structure. However, the accuracy could still be further enhanced in the future by supplying a much large amount of data, as well as using a deeper neural network.

Table 1 shows the advantages and disadvantages of the proposed VOC detection and existing state-of-the-art. Compared with the current VOC sensors (chemi-resistive, semi-conductor, and frequency-based) in references [96–100], the proposed ML-enhanced VOC plasma discharge sensors show both superfast response (millisecond) and recovery. In addition, our sensor can detect the multi-VOCs without any external power sources, which is suitable for applications in IoT. Compared with the ion mobility sensors in reference [3,23,101], we found that the ML-enhanced VOC plasma discharge sensors showed relative tolerance in the environment, such as the detection in RT and air pressure, whereas the other method is unreachable. It also proposes atmospheric low-temperature plasma driven by TENG, whereas plasma discharge from other power sources was impossible with such low temperature in operation. Further, the conventional method resulting a large size of the system makes it impossible to fit the applications in the IoT and with the ability of portability.

4. Conclusion

In summary, we proposed an ML-enhanced VOC concentration detecting method using an SM-TENG-enabled ion mobility analyzer based on the multi-switched manipulation, which well solved the weaknesses of existing plasma discharge systems, i.e., bulky, high-temperature operation, and inappropriate for VOC concentration detection. With the aid of the charge accumulation mechanism, the SM-TENG could provide a high output voltage at the order of ~600 V, which was difficult to be achieved by the conventional TENG. With certain tip-plate electrode configurations, the voltage from SM-TENG was leveraged as the power source to obtain plasma discharge patterns of various VOCs with different ion mobility characteristics. We observed that the discharge pattern for each VOC mixture was unique and repeatable, which could be considered a strong basis for distinguishing different gases. To improve the detection accuracy of the system for VOC monitoring, an ML-enhanced tool was demonstrated to classify different VOC concentrations based on specific features extracted automatically from the ion mobility spectrometry data with an accuracy of 48.214%, which is reasonable considering the properties of gas molecules. Moreover, the dependence between the transient time-domain and the gap distance in needle-plate configuration was discussed for air discharge to validate the robustness of the ML-enhanced method, and an accuracy of 54.286% was obtained with the gap distance of ~2 mm. It demonstrated that the proposed multi-switched manipulation platform enables the detection of various VOC species (methanol, ethanol, acetone, and IPA) with the aid of AI technology, showing a portable real-time VOC-monitoring solution with a rapid response and low power consumption for future IoT-based environmental monitoring applications.

Conflict of interest

The authors declare that they have no conflict of interest.

Acknowledgments

This work was supported by the research grant of "Chip-Scale MEMS Micro-Spectrometer for Monitoring Harsh Industrial Gases" (R-263-000-C91-305) at the National University of Singapore (NUS), Singapore; and the research grant of RIE Advanced Manufacturing and Engineering (AME) programmatic grant A18A4b0055 "Nanosystems at the Edge" at NUS, Singapore.

Author contributions

Jianxiong Zhu conceived and designed the project, and wrote the manuscript. Zhongda Sun did the software about machine learning. Jikai Xu did data curation. Rafal D. Walczak and Jan A Dziuban advised on data analysis. Chengkuo Lee supervised the whole research. All the authors contributed extensively to the work presented in this paper.

Appendix A. Supplementary materials

Supplementary materials to this article can be found online at https://doi.org/10.1016/j.scib.2021.03.021.

References

[1] Consales M, Cutolo A, Penza M, et al. Carbon nanotubes coated acoustic and optical VOCs sensors: towards the tailoring of the sensing performances. IEEE Trans Nanotechnol 2007;6:601–12.
[2] Gesemann B, Wehrspohn R, Hackner A, et al. Large-scale fabrication of ordered silicon nanotip arrays used for gas ionization in ion mobility spectrometers. IEEE Trans Nanotechnol 2011;10:50–2.
[3] Michalczuk B, Moravský L, Hrdá J, et al. Atmospheric pressure chemical ionisation study of selected volatile organic compounds (VOCs) by ion mobility spectrometry coupled with orthogonal acceleration time of flight mass spectrometry. Int J Mass Spectrom 2020;449:116275.
[4] Broza YY, Zhou X, Yuan M, et al. Disease detection with molecular biomarkers: from chemistry of body fluids to nature-inspired chemical sensors. Chem Rev 2019;119:11761–817.
[5] Zhao K, Gu G, Zhang Y, et al. The self-powered CO_2 gas sensor based on gas discharge induced by triboelectric nanogenerator. Nano Energy 2018;53:898–905.
[6] Cho I, Kang K, Yang D, et al. Localized liquid-phase synthesis of porous SnO_2 nanotubes on MEMS platform for low-power, high performance gas sensors. ACS Appl Mater Interfaces 2017;9:27111–9.
[7] Cho M, Zhu J, Kim H, et al. Half-pipe palladium nanotube-based hydrogen sensor using a suspended nanofiber scaffold. ACS Appl Mater Interfaces 2019;11:13343–9.
[8] Hasan D, Lee C. Hybrid metamaterial absorber platform for sensing of CO_2 gas at mid-IR. Adv Sci 2018;5:1700581.
[9] Chang Y, Hasan D, Dong B, et al. All-dielectric surface-enhanced infrared absorption-based gas sensor using guided resonance. ACS Appl Mater Interfaces 2018;10:38272–9.
[10] Matatagui D, Sainz-Vidal A, Gràcia I, et al. Chemoresistive gas sensor based on ZIF-8/ZIF-67 nanocrystals. Sens Actuators B Chem 2018;274:601–8.
[11] Zhu J, Cho M, Li Y, et al. Biomimetic turbinate-like artificial nose for hydrogen detection based on 3D porous laser-induced graphene. ACS Appl Mater Interfaces 2019;11:24386–94.
[12] Manesh KM, Gopalan A, Lee K, et al. Fabrication of functional nanofibrous ammonia sensor. IEEE Trans Nanotechnol 2007;6:513–8.
[13] Abdellah A, Abdelhalim A, Horn M, et al. Scalable spray deposition process for high-performance carbon nanotube gas sensors. IEEE Trans Nanotechnol 2013;12:174–81.
[14] Rahman R, Servati P. Efficient analytical model of conductivity of CNT/polymer composites for wireless gas sensors. IEEE Trans Nanotechnol 2015;14:118–29.
[15] Vautz W, Franzke J, Zampolli S, et al. On the potential of ion mobility spectrometry coupled to GC pre-separation – a tutorial. Anal Chim Acta 2018;1024:52–64.
[16] Bohrer B, Merenbloom S, Koeniger S, et al. Biomolecule analysis by ion mobility spectrometry. Annu Rev Anal Chem 2008;1:293–327.
[17] Zheng X, Wojcik R, Zhang X, et al. Coupling front-end separations, ion mobility spectrometry, and mass spectrometry for enhanced multidimensional biological and environmental analyses. Annu Rev Anal Chem 2017;10:71–92.
[18] Bocos-Bintintan V, Thomas C, Ratiu I. Sensors' array of aspiration ion mobility spectrometer as a tool for bacteria discrimination. Talanta 2020;206:120233.
[19] Puton J, Namieśnik J. Ion mobility spectrometry: current status and application for chemical warfare agents detection. Trac-Trend Anal Chem 2016;85:10–20.
[20] Kabir K, Donald W. Microscale differential ion mobility spectrometry for field deployable chemical analysis. Trac-Trend Anal Chem 2017;97:399–427.
[21] Chen C, Jiang D, Li H. UV photoionization ion mobility spectrometry: fundamentals and applications. Anal Chim Acta 2019;1077:1–13.
[22] Cheng G, Zheng H, Yang F, et al. Managing and optimizing the output performances of a triboelectric nanogenerator by a self-powered electrostatic vibrator switch. Nano Energy 2018;44:208–16.
[23] Jünger M, Bödeker B, Baumbach J. Peak assignment in multi-capillary column—ion mobility spectrometry using comparative studies with gas chromatography—mass spectrometry for VOC analysis. Anal Bioanal Chem 2010;396:471–82.
[24] Wang S, Chen H, Sun B. Recent progress in food flavor analysis using gas chromatography–ion mobility spectrometry (GC–IMS). Food Chem 2020;315:126158.
[25] Mochalski P, Wiesenhofer H, Allers M, et al. Monitoring of selected skin- and breath-borne volatile organic compounds emitted from the human body using gas chromatography ion mobility spectrometry (GC-IMS). J Chromatogr B 2018;1076:29–34.
[26] Grzebyk T, Górecka-Drzazga A. MEMS type ionization vacuum sensor. Sens Actuators A Phys 2016;246:148–55.
[27] Stark R, Schoenbach K. MEMS type ionization vacuum sensor. J Appl Phys 1999;85:2075.
[28] Liu H, Fu H, Sun L, et al. Hybrid energy harvesting technology from materials, structural design, system integration to applications. Renew Sustain Energy Rev 2021;137:110473.
[29] Hu W, Wan L, Jian Y, et al. Electronic noses: from advanced materials to sensors aided with data processing. Adv Mater Technol 2019;4:1800488.
[30] Wang S, Lin L, Wang Z. Triboelectric nanogenerators as self-powered active sensors. Nano Energy 2015;11:436.
[31] Zhang C, Wang Z. Tribotronics—a new field by coupling triboelectricity and semiconductor. Nano Today 2016;11:521.
[32] Fan F, Tian Z, Wang Z. Flexible triboelectric generator. Nano Energy 2012;1:328.
[33] Niu S, Liu Y, Wang S, et al. Theory of sliding-mode triboelectric nanogenerators. Adv Mater 2013;25:6184.
[34] Niu S, Wang Z. Theoretical systems of triboelectric nanogenerators. Nano Energy 2015;14:161–92.
[35] Kwon Y, Shin S, Kim Y, et al. Triboelectric contact surface charge modulation and piezoelectric charge inducement using polarized composite thin film for performance enhancement of triboelectric generators. Nano Energy 2016;25:225.
[36] Khan A, Mahmud A, Ban D. Evolution from single to hybrid nanogenerator: a contemporary review on multimode energy harvesting for self-powered electronics. IEEE Trans Nanotechnol 2019;18:21–36.
[37] Zou H, Zhang Y, Guo L, et al. Quantifying the triboelectric series. Nat Commun 2019;10:1427.
[38] Wang Z, Chen J, Lin L. Progress in triboelectric nanogenerators as a new energy technology and self-powered sensors. Energy Environ Sci 2015;8:2250–82.
[39] Hinchet R, Yoon H, Ryu H, et al. Transcutaneous ultrasound energy harvesting using capacitive triboelectric technology. Science 2019;365:491–4.
[40] Kim S, Gupta M, Lee K, et al. Transparent flexible graphene triboelectric nanogenerators. Adv Mater 2014;26:3918–25.
[41] Khan U, Kim T, Ryu H, et al. Graphene tribotronics: graphene tribotronics for electronic skin and touch screen applications. Adv Mater 2017;29:1.
[42] Seung W, Yoon H, Kim T, et al. Boosting power-generating performance of triboelectric nanogenerators via artificial control of ferroelectric polarization and dielectric properties. Adv Energy Mater 2017;7:1600988.
[43] Zhong J, Zhong Q, Fan F, et al. Finger typing driven triboelectric nanogenerator and its use for instantaneously lighting up LEDs. Nano Energy 2013;2:491–7.
[44] Cheng X, Miao L, Song Y, et al. High efficiency power management and charge boosting strategy for a triboelectric nanogenerator. Nano Energy 2017;38:438–46.
[45] Vasandani P, Gattu B, Mao Z, et al. Using a synchronous switch to enhance output performance of triboelectric nanogenerators. Nano Energy 2018;43:210–8.
[46] Chun J, Ye B, Lee J, et al. Boosted output performance of triboelectric nanogenerator via electric double layer effect. Nat Commun 2016;7:12985.
[47] Xu L, Wu H, Yao G, et al. Giant voltage enhancement via triboelectric charge supplement channel for self-powered electroadhesion. ACS Nano 2018;12:10262–71.
[48] Qin H, Cheng G, Zi Y, et al. High energy storage efficiency triboelectric nanogenerators with unidirectional switches and passive power management circuits. Adv Funct Mater 2018;28:1805216.
[49] Xiao T, Jiang T, Zhu J, et al. Silicone-based triboelectric nanogenerator for water wave energy harvesting. ACS Appl Mater Interfaces 2018;10:3616–23.
[50] Zhu J, Zhu Y, Song W, et al. Zinc oxide enhanced piezoelectret polypropylene microfibers for mechanical energy harvesting. ACS Appl Mater Interfaces 2018;10:19940–7.
[51] He T, Wang H, Wang J, et al. Self-sustainable wearable textile nano-energy nano-system (NENS) for next-generation healthcare applications. Adv Sci 2019;6:1901437.
[52] Zhu J, Liu X, Shi Q, et al. Development trends and perspectives of future sensors and MEMS/NEMS. Micromachines 2020;11:541.
[53] Ryu H, Lee J, Khan U, et al. Sustainable direct current powering a triboelectric nanogenerator via a novel asymmetrical design. Energy Environ Sci 2018;11:2057.
[54] He C, Han C, Gu G, et al. Hourglass triboelectric nanogenerator as a "direct current" power source. Adv Energy Mater 2017;7:1700644.
[55] Luo J, Xu L, Tang W, et al. Direct-current triboelectric nanogenerator realized by air breakdown induced ionized air channel. Adv Energy Mater 2018;8:1800889.
[56] Liu D, Yin X, Guo H, et al. A constant current triboelectric nanogenerator arising from electrostatic breakdown. Sci Adv 2019;5:6437.
[57] Koh K, Shi Q, Cao S, et al. A self-powered 3D activity inertial sensor using hybrid sensing mechanisms. Nano Energy 2019;56:651–61.
[58] Shi Q, Qiu C, He T, et al. Triboelectric single-electrode-output control interface using patterned grid electrode. Nano Energy 2019;60:545–56.
[59] Shi Q, Zhang Z, Chen T, et al. Minimalist and multi-functional human machine interface (HMI) using a flexible wearable triboelectric patch. Nano Energy 2019;62:355–66.
[60] Yang J, Yang F, Zhao L, et al. Managing and optimizing the output performances of a triboelectric nanogenerator by a self-powered electrostatic vibrator switch. Nano Energy 2018;46:220–8.
[61] Chen H, Miao L, Su Z, et al. Fingertip-inspired electronic skin based on triboelectric sliding sensing and porous piezoresistive pressure detection. Nano Energy 2017;40:65–72.

[62] Yang H, Pang Y, Bu T, et al. Triboelectric micromotors actuated by ultralow frequency mechanical stimuli. Nat Commun 2019;10:2309.
[63] Wang J, He T, Lee C. Development of neural interfaces and energy harvesters towards self-powered implantable systems for healthcare monitoring and rehabilitation purposes. Nano Energy 2019;65:104039.
[64] Shi Q, Lee C. Self-powered bio-inspired spider-net-coding interface using single-electrode triboelectric nanogenerator. Adv Sci 2019;6:1900617.
[65] Wang H, Wang J, He T, et al. Direct muscle stimulation using diode amplified triboelectric nanogenerators (TENGs). Nano Energy 2019;63:103844.
[66] Zhu J, Guo X, Meng D, et al. A flexible comb electrode triboelectric-electret nanogenerator with separated microfibers for self-powered position, motion direction and acceleration tracking sensor. J Mater Chem A 2018;6:16548–55.
[67] Dhakar L, Pitchappa P, Tay F, et al. An intelligent skin based self-powered finger motion sensor integrated with triboelectric nanogenerator. Nano Energy 2016;19:532–40.
[68] Wu C, Liang Y, Hu W, et al. Interface-regulated contact electrification for power-free and highly selective gas sensing. Adv Intell Syst 2019;1:1900066.
[69] Su Y, Yang T, Zhao X, et al. A wireless energy transmission enabled wearable active acetone biosensor for non-invasive prediabetes diagnosis. Nano Energy 2020;74:104941.
[70] Su Y, Wang J, Wang B, et al. Alveolus-inspired active membrane sensors for self-powered wearable chemical sensing and breath analysis. ACS Nano 2020;14:6067–75.
[71] Huang C, Chen G, Nashalian A, et al. Advances in self-powered chemical sensing via a triboelectric nanogenerator. Nanoscale 2021;13:2065–81.
[72] Wen Z, Chen J, Yeh M, et al. Blow-driven triboelectric nanogenerator as an active alcohol breath analyzer. Nano Energy 2015;16:38–46.
[73] Dong B, Shi Q, Yang Y, et al. Technology evolution from self-powered sensors to AIoT enabled smart homes. Nano Energy 2021;79:105414.
[74] Liu F, Liu Y, Lu Y, et al. Electrical analysis of triboelectric nanogenerator for high voltage applications exampled by DBD microplasma. Nano Energy 2019;56:482–93.
[75] Cheng G, Zheng H, Yang F, et al. Managing and maximizing the output power of a triboelectric nanogenerator by controlled tip–electrode air-discharging and application for UV sensing. Nano Energy 2018;44:208–16.
[76] Li A, Zi Y, Guo H, et al. Triboelectric nanogenerators for sensitive nano-coulomb molecular mass spectrometry. Nat Nanotechnol 2017;12:481.
[77] Cheng J, Ding W, Zi Y, et al. Triboelectric microplasma powered by mechanical stimuli. Nat Commun 2018;9:3733.
[78] Wang J, Wu C, Dai Y, et al. Achieving ultrahigh triboelectric charge density for efficient energy harvesting. Nat Commun 2017;8:88.
[79] Wang J, Li S, Yi F, et al. Sustainably powering wearable electronics solely by biomechanical energy. Nat Commun 2016;7:12744.
[80] Liu D, Zhou L, Li S, et al. Hugely enhanced output power of direct-current triboelectric nanogenerators by using electrostatic breakdown effect. Adv Mater Technol 2020;5:2000289.
[81] Zhou Z, Chen K, Li X, et al. Sign-to-speech translation using machine-learning-assisted stretchable sensor arrays. Nat Electron 2020;3:571–8.
[82] Meng K, Zhao S, Zhou Y, et al. A wireless textile-based sensor system for self-powered personalized health care. Matter 2020;2:896–907.
[83] Zhou Z, Padgett S, Cai Z, et al. Single-layered ultra-soft washable smart textiles for all-around ballistocardiograph, respiration, and posture monitoring during sleep. Biosens Bioelectron 2020;155:112064.
[84] Tat T, Libanori A, Au C, et al. Advances in triboelectric nanogenerators for biomedical sensing. Biosens Bioelectron 2021;171:112714.
[85] Zou Y, Raveendran V, Chen J. Wearable triboelectric nanogenerators for biomechanical energy harvesting. Nano Energy 2020;77:105303.
[86] Chen T, Zhao M, Shi Q, et al. Novel augmented reality interface using a self-powered triboelectric based virtual reality 3D-control sensor. Nano Energy 2018;51:162–72.
[87] Chen J, Xuan W, Zhao P, et al. Triboelectric effect based instantaneous self-powered wireless sensing with self-determined identity. Nano Energy 2018;51:1–9.
[88] Qiu C, Wu F, Shi Q, et al. Sensors and control interface methods based on triboelectric nanogenerator in IoT applications. IEEE Access 2019;7:92745–57.
[89] Zhu J, Wang H, Zhang Z, et al. Continuous direct current by charge transportation for next-generation IoT and real-time virtual reality applications. Nano Energy 2020;73:104760.
[90] Wen F, Sun Z, He T, et al. Machine learning glove using self-powered conductive superhydrophobic triboelectric textile for gesture, recognition in VR/AR applications. Adv Sci 2020;7:2000261.
[91] Shi Q, Dong B, He T, et al. Progress in wearable electronics/photonics – moving towards the era of artificial intelligence (AI) and internet of things (IoT). InfoMat 2020;2:1131–62.
[92] Zhu M, Sun Z, Zhang Z, et al. Haptic-feedback smart glove as a creative human machine interface (HMI) for virtual/augmented reality applications. Sci Adv 2020;6:eaaz8693.
[93] Zhu J, Ren Z, Lee C. Toward healthcare diagnoses by machine-learning-enabled volatile organic compound identification. ACS Nano 2021;15:894–903.
[94] Wang H, Zhu J, He T, et al. Programmed-triboelectric nanogenerators—a multi-switch regulation methodology for energy manipulation. Nano Energy 2020;78:105241.
[95] Gasan D, Zhu J, Wang H, et al. Feasibility study of high-voltage ion mobility for gas identification based on triboelectric power source. In: 2019 19th international conference on micro and nanotechnology for power generation and energy conversion applications (PowerMEMS), Krakow, Poland. p. 1–5.
[96] Kida T, Suematsu K, Hara K, et al. Ultrasensitive detection of volatile organic compounds by a pore tuning approach using anisotropically shaped SnO_2 nanocrystals. ACS Appl Mater Interfaces 2016;8:35485–95.
[97] Perfecto T, Zito C, Volanti D. Room-temperature volatile organic compounds sensing based on $WO_3{\cdot}0.33H_2O$, hexagonal-WO_3 and their reduced graphene oxide composites. RSC Adv 2016;6:105171.
[98] Kim J, Yoo H, Choi H, et al. Tunable volatile organic compounds sensor by using thiolated ligand conjugation on MoS_2. Nano Lett 2014;14:5941–7.
[99] Liu B, Huang Y, Kam K, et al. Functionalized graphene-based chemiresistive electronic nose for discrimination of disease-related volatile organic compounds. Biosens Bioelectron X 2019;1:100016.
[100] Bao Y, Xu P, Cai S, et al. Detection of volatile-organic-compounds (VOCs) in solution using cantilever-based gas sensors. Talanta 2018;182:148–55.
[101] Cheng S, Li H, Jiang D, et al. Sensitive detection of trimethylamine based on dopant-assisted positive photoionization ion mobility spectrometry. Talanta 2017;162:398–402.

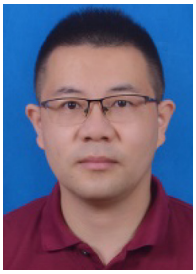

Jianxiong Zhu is currently an associate professor at Southeast University, China. He is also doing postdoc at the Department of Electrical and Computer Engineering, the National University of Singapore. He received his B. Eng. degree in Electrical and Automation Engineering from the Hubei University of Technology in 2006. After that, he got his Master's degree from the University of Science and Technology of China and Ph.D. degree from the University of Missouri Columbia in 2015. His research interest is focused on MEMS zero-power sensor, wearable flexible sensor, and gas sensor.

Chengkuo Lee received his Ph.D. degree in Precision Engineering from The University of Tokyo in 1996. Currently, he is the director of the Center for Intelligent Sensors and MEMS at the National University of Singapore, Singapore. He specializes in sensors, micro- and nanoelectromechanical systems.